

# Role of Defects in the Nucleation and Growth of Au Nanoclusters on SiO<sub>2</sub> Thin Films

B. K. Min, W. T. Wallace, A. K. Santra, and D. W. Goodman\*

Department of Chemistry, Texas A&M University, P.O. Box 30012, College Station, Texas 77842-3012

Received: August 3, 2004; In Final Form: September 14, 2004

Scanning tunneling microscopy (STM), in conjunction with the nucleation and growth of Au clusters, has been used to identify and quantify various types of defects on ordered, SiO<sub>2</sub> thin films grown on Mo(112). On a low-defect surface, Au clusters nucleate and grow at line defects with metal deposition at room temperature, whereas deposition at 850 K leads to cluster decoration primarily at step edges. On a highly defective surface, clusters nucleate and grow at point defects (oxygen vacancies and/or oxygen vacancy complexes) on the terraces, with some clusters grown on oxygen vacancy complexes remaining even after an 850 K anneal. The average cluster density for low Au coverages deposited at room temperature is identical to that obtained for the same Au coverage deposited at 850 K, consistent with complete titration of point defects by the nucleating clusters.

## I. Introduction

The growth of metals on oxide surfaces is important in numerous technologies including electronic device fabrication and heterogeneous catalysis.<sup>1</sup> With respect to the latter, the activity and selectivity of metal-catalyzed reactions are often sensitive to the metal particle morphology. For example, the catalytic activity of Au supported on certain oxides depends critically on the morphology of the clusters.<sup>2</sup> In general, the morphology of metal particles on oxide surfaces depends to a large extent on defects, particularly point defects such as oxygen vacancies.<sup>3–8</sup> Several studies have addressed the relationship between metal cluster nucleation/growth on oxide surfaces and defects; however, many questions remain unanswered. Most recently, a study by Besenbacher and co-workers using scanning tunneling microscopy (STM) showed that bridging oxygen vacancies on TiO<sub>2</sub> are active nucleation sites for Au clusters.<sup>3</sup> In addition, these authors suggested that the diffusion of a vacancy-cluster complex plays an important role in the formation of larger Au clusters. Using atomic force microscopy (AFM), Barth and co-workers have quantified point defects on MgO by estimating the Pd cluster density as a function of the deposition surface temperature.<sup>4</sup> In a theoretical study, Bogicevic and Jennison have calculated the binding energies of various metals to MgO and showed that dimers of noble metals are more stable at oxygen vacancies.<sup>5</sup> Using STM, Freund and co-workers have demonstrated preferential decoration of Pd and Rh metal particles on line defects of Al<sub>2</sub>O<sub>3</sub>.<sup>6,7</sup> Very recently, defects on crystalline SiO<sub>2</sub> thin films have been studied in our laboratory using ultraviolet photoelectron spectroscopy (UPS) and metastable impact electron spectroscopy techniques (MIES).<sup>9</sup>

In this study we demonstrate that Au clusters nucleate and grow at defect sites on SiO<sub>2</sub> thin films. Consequently, the nucleation and growth of the Au clusters allow assessment of the defect density and type.

## II. Experimental Section

All experiments were carried out in an UHV chamber with a base pressure of  $5 \times 10^{-10}$  Torr; details of the apparatus have been described elsewhere.<sup>10</sup> Typically, the STM images were acquired in the constant current mode at 1–2 V and  $\sim 0.1$  nA. Ultrahigh purity (99.999%) oxygen from MG industries and a Mo(112) crystal oriented to  $<0.25^\circ$  (from Matek, Germany) were used for the study. The Mo(112) crystal was cleaned by oxygen treatment and high-temperature annealing (2100 K) until no traces of carbon and oxygen were evident by Auger electron spectroscopy (AES). The Au coverage was determined using calibration data of Au/Mo AES ratios versus Au coverage. The Au coverage on the SiO<sub>2</sub> thin films was determined by measuring the total volume of the Au particles, showing that the coverage on the films is consistent with the AES-determined coverage within 6%. A thermocouple (W-5%Re/W-26%Re) was used to measure the surface temperature and to calibrate an optical pyrometer (OMEGA OS3700) prior to disconnection for the STM measurements. The pyrometer was then used to measure the temperature in subsequent annealing experiments.

## III. Results and Discussion

Ordered, ultrathin SiO<sub>2</sub> films with a thickness of  $0.35 \pm 0.05$  nm were synthesized by vapor deposition of Si onto a  $p(2 \times 3)$ -O reconstructed surface of Mo(112), oxidation at 800 K, and an anneal in oxygen at 1100–1200 K.<sup>11</sup> The resulting SiO<sub>2</sub> thin film shows a very flat, homogeneous structure with STM, a wide band gap with UPS and MIES,<sup>12</sup> and very sharp  $c(2 \times 2)$  diffraction features in low energy electron diffraction (LEED).<sup>13</sup> The method of preparation and structural characterization of the film are described in detail elsewhere.<sup>11,13</sup>

Frequently, defects play a key role in the nucleation and growth of metals on oxide surfaces, and in the electronic and chemical properties of metal-oxide systems.<sup>14</sup> Defects on oxide surfaces are usually classified as extended defects (e.g., steps), line defects (e.g., antiphase domain boundaries<sup>15</sup>), and point defects (e.g., oxygen vacancies<sup>16</sup>). Defects in the SiO<sub>2</sub> film are

\* To whom correspondence should be addressed. E-mail: goodman@mail.chem.tamu.edu.

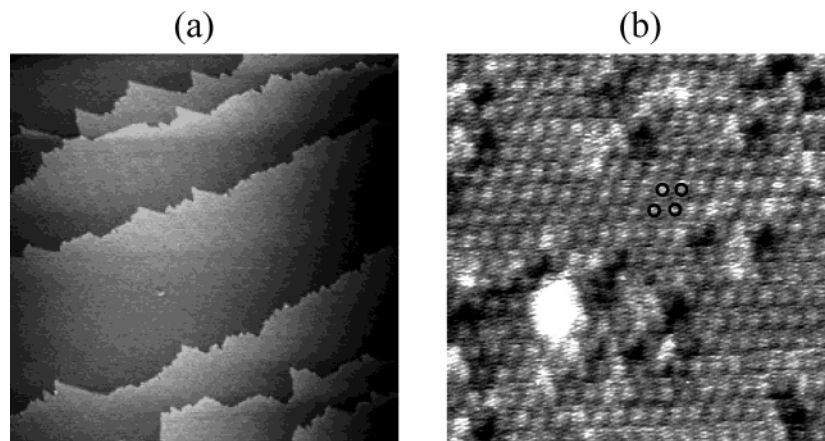


**Figure 1.** STM images of a 1200 K annealed  $\text{SiO}_2$  thin film ( $U_T = 2.0$  V and  $I = 0.1$  nA) (a)  $200 \text{ nm} \times 200 \text{ nm}$ , (b)  $10 \text{ nm} \times 10 \text{ nm}$ , atomic corrugations with a  $c(2 \times 2)$  array are represented by black circles.

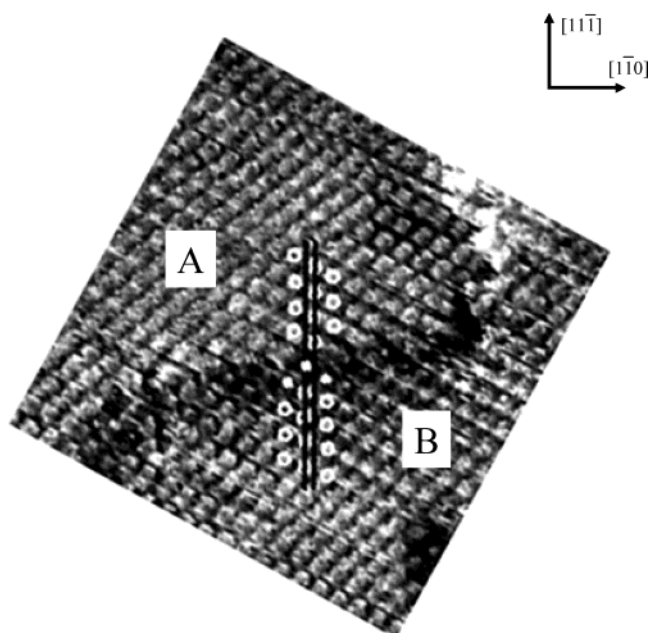


**Figure 2.** A  $10 \text{ nm} \times 10 \text{ nm}$  STM image with the  $c(2 \times 2)$  structure highlighted by white circles. Areas A and B indicate two different domains separated by a line defect.

evident in the STM images of Figure 1. The steps separating the terraces in the STM image of Figure 1a originate from the Mo(112) substrate. In the higher resolution STM image of Figure 1b, the  $c(2 \times 2)$  structure of the substrate is indicated by small, black open circles. The lattice spacing between adjacent atoms of the  $c(2 \times 2)$  atomic array is  $\sim 0.5$  nm, essentially the same as that found by LEED (0.52 nm). In addition to this  $c(2 \times 2)$  atomic corrugation, some dark contrast spots with one atomic corrugation size are also seen in the STM image.

A line-type feature with sharp contrast along the  $[1, -1, 0]$  direction is apparent in the STM image of Figure 2. Close inspection shows that the white circles, drawn coincident with the atomic corrugations on both sides of the line-type feature, are out-of-registry with respect to each other, with a mismatch of approximately 0.22 nm. This mismatch is equal to one-half the distance between two Mo atomic rows (0.445 nm) in the  $[1, -1, 0]$  direction, and therefore likely due to two domains of  $\text{SiO}_2$ . That line defects in  $\text{SiO}_2$  thin films on Mo(112) arise due to antiphase domain boundaries has previously been suggested by Freund and co-workers on the basis of the significant broadening of the superlattice spots in LEED.<sup>18,19</sup> Also, very

recently, line defects on an  $\text{Al}_2\text{O}_3$  thin film grown on NiAl(110) arising from antiphase domain boundaries was reported by Kulawik and co-workers.<sup>15</sup> A precise structure of this line-type defect is not possible because of the limited resolution of the STM images.

The STM images in Figure 3a,b show the morphologies of  $\text{SiO}_2$ -supported clusters grown at room temperature (RT) with Au coverages of 0.10 and 0.40 monolayer (ML), respectively. At 0.10 ML the Au clusters nucleate at terrace and step edge sites with no apparent orientation of the clusters with respect to the substrate. However, the Au clusters grown at 0.40 ML (Figure 3b) are aligned along the  $[1, -1, 0]$  direction, consistent with nucleation and growth along line defects. The decoration of line defects with metal clusters has been observed previously for Pd and Rh clusters grown on  $\text{Al}_2\text{O}_3$  thin films.<sup>6,7</sup> Au cluster growth was essentially independent of the rate of metal deposition (see Figure 3c), consistent with heterogeneous cluster nucleation. Cluster growth at a surface temperature of 850 K (Figure 3d) shows that step edges, rather than line defects, are decorated, implying that step edges are more stable sites for cluster nucleation and growth.

To investigate the influence of oxygen vacancies on cluster nucleation, a  $\text{SiO}_2$  film with a relatively high density of defects was prepared using an anneal temperature of 1100 K. Although the film annealed at 1100 K yielded very similar LEED, AES, and STM data as for a 1200 K annealed film, the growth of Au clusters was dramatically different, as can be seen in Figure 4a–d. Whereas on a low-defect (1150–1200 K annealing temperature)  $\text{SiO}_2$  film the Au clusters align along line defects, on the high-defect film ( $< 1150$  K annealing), the clusters nucleate primarily on terrace sites. Also on the low-defect film, clusters nucleate extensively at step edges, in contrast to little step-edge decoration for the high-defect film. To test further whether nucleation and growth of Au nanoclusters correlates with the point defect density, the nucleation and growth of Au clusters was carried out at a relatively high surface temperature (850 K). The results are shown in Figure 4d where the number density of Au clusters is similar to that for nucleation and growth at room temperature (Figure 4a).

Although the precise nature of the point defects on our films is uncertain, the most probable species are oxygen vacancies. Chemical defects such as silanol groups are unlikely because our films are annealed to at least 1100 K, well above the temperature at which such species are stable.<sup>18,20</sup> In addition, no hydroxyl features are observed in the as-prepared films by high-resolution electron energy loss spectroscopy (HREELS).

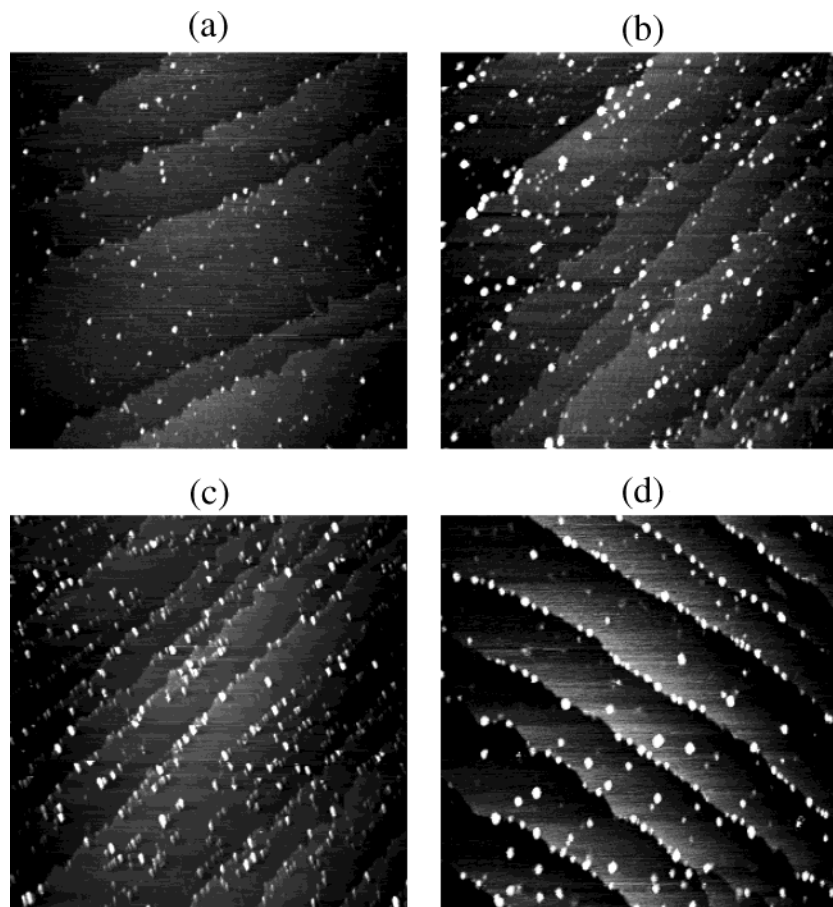


**Figure 3.** STM images ( $200 \text{ nm} \times 200 \text{ nm}$ ,  $U_T = 1.8 \text{ V}$  and  $I = 0.08 \text{ nA}$ ) of Au clusters on a 1200 K annealed  $\text{SiO}_2$  film after deposition of (a) 0.10 ML of Au at 0.010 ML/min, surface temperature of 300 K; (b) 0.40 ML of Au at 0.010 ML/min, surface temperature of 300 K; (c) 0.33 ML of Au at 0.033 ML/min, surface temperature of 300 K; and (d)  $\sim 0.4$  ML at 0.010 ML/min, surface temperature of 850 K.

To further test the stability of the various defect sites, different coverages of Au were deposited on a highly defective  $\text{SiO}_2$  surface followed by an anneal to 850 K. The number densities of Au clusters obtained at each state are shown in Figure 5. For the 0.2, 0.7, and 1.3 ML Au coverages, the number densities after an anneal to 850 K show constant values irrespective of Au coverage. Additionally, the cluster number density present upon deposition of 0.6 ML Au at a surface temperature of 850 K is indicated at the right of the figure. As can be seen, the density at this deposition temperature is similar to that after the other coverages have been annealed. These data indicate the saturation of especially stable nucleation points on the terraces.

The average cluster density as a function of Au coverage, estimated from the STM images of several scanned areas, is shown in Figure 6. This figure shows three distinct regions corresponding to Au coverages of  $<0.17$ ,  $0.17\text{--}0.33$ , and  $>0.33$  ML. Up to  $\sim 0.17$  ML the cluster density is essentially independent of the Au coverage. The cluster density rapidly increases between  $\sim 0.17$  and 0.33 ML, after which the cluster density remains essentially constant.

These results suggest that the low coverage region with a constant density of Au clusters correlates with the number of point defects (oxygen vacancies). However, the precise number of neighboring oxygen vacancies required for nucleation and growth of clusters is difficult to assess. According to Besenbacher and co-workers, single oxygen vacancies on  $\text{TiO}_2$  bind approximately three Au atoms, whereas larger Au clusters

require several oxygen vacancies.<sup>3</sup> According to this model, the number of Au atoms in a 1.4 nm cluster is  $\sim 20$  and would require  $\sim 7$  oxygen vacancies.

As seen in Figure 6, the density of Au clusters above 0.1 ML increases and saturates between 0.3 and 0.6 ML. The increase in cluster density from 0.1 to 0.3 ML indicates that there are nucleation sites in addition to the point defects described above. After reaching saturation, the Au cluster density is essentially constant whereas the average cluster size increases. This suggests that deposited adatoms are captured by existing Au clusters within the saturation coverage range up to 1.3 ML.

Finally, on the basis of our STM observations, the relative stability of Au nanoclusters on various defect sites can be estimated. As seen in Figure 4d, Au clusters do not preferentially decorate step edge sites even during deposition at a high surface temperature. Therefore, point defects with several oxygen vacancies (oxygen vacancy complexes)<sup>21</sup> are more stable for cluster growth than step edges. In addition, as mentioned previously, step edges are more stable sites than line defects for cluster growth (Figure 3d). It should be noted that cluster growth related to point defects disappears upon an anneal to 1150–1200 K in an oxygen environment and cluster nucleation changes to decoration of line defects, although oxygen vacancies are still expected to be present. However, most vacancies are single oxygen vacancies and therefore do not play a role as active nucleation and growth sites for Au clusters. These do, however, compete with line defects, which are more stable sites for Au nanoclusters. On the basis of these results, the stability

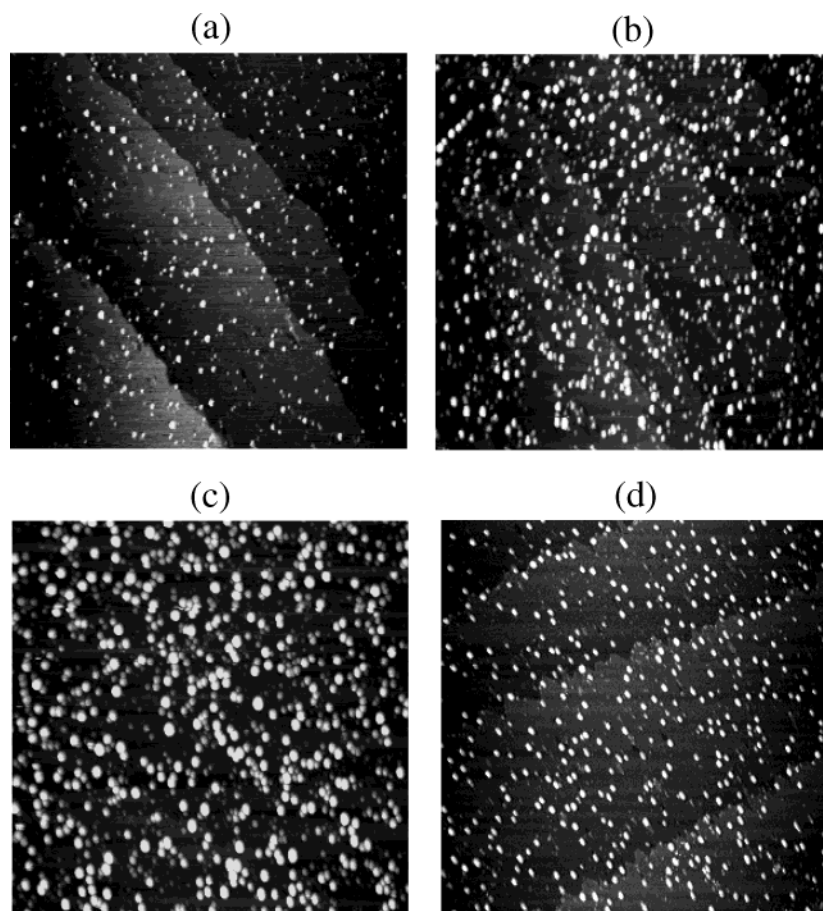


**Figure 4.** STM images ( $200 \text{ nm} \times 200 \text{ nm}$ ,  $U_T = 1.8 \text{ V}$  and  $I = 0.08 \text{ nA}$ ) of Au clusters on a 1100 K annealed  $\text{SiO}_2$  film after deposition of (a) 0.17 ML of Au at 0.033 ML/min, surface temperature of 300 K; (b) 0.33 ML of Au at 0.033 ML/min, surface temperature of 300 K; (c) 1.32 ML of Au at 0.033 ML/min, surface temperature of 300 K; and (d)  $\sim 0.3 \text{ ML}$  of Au at 0.033 ML/min, surface temperature of 850 K.

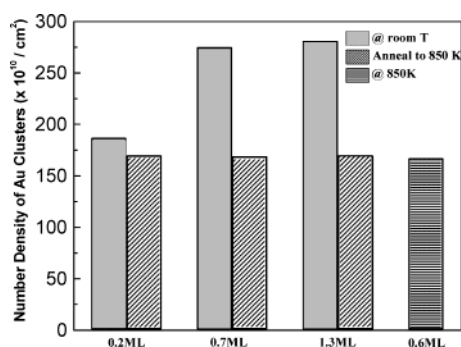


**Figure 5.** Bar graph representation of the average cluster number density on a highly defective  $\text{SiO}_2$  surface under different Au coverages. For 0.2, 0.7, and 1.3 ML Au coverages, the cluster density both before and after an anneal to 850 K are shown. For 0.6 ML Au coverage, the cluster density obtained upon deposition at a surface temperature of 850 K is shown. The constant cluster densities obtained by annealing to 850 K or depositing at 850 K indicate the saturation of especially stable nucleation sites on the terraces.

of Au nanoclusters on various defect sites is anticipated to be (from high to low): oxygen vacancy complexes > step edges > line defects > single oxygen vacancies.

#### IV. Conclusions

On the basis of our STM studies, Au nanoclusters can be used to highlight defects on  $\text{SiO}_2$  thin films with cluster growth related to a specific defect feature. On a well-prepared  $\text{SiO}_2$  thin film, Au nanoclusters preferentially decorate line defects.

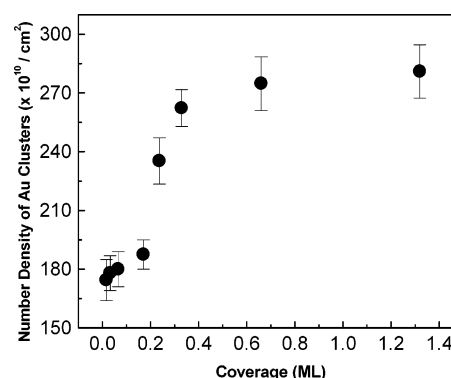


**Figure 6.** Plot showing the Au cluster densities obtained as a function of Au coverage on a highly defective  $\text{SiO}_2$  film upon deposition at room temperature. Three distinct regions can be seen, which correspond to Au coverages of less than 0.17 ML, between 0.17 and 0.33 ML, and greater than 0.33 ML.

However, higher densities of Au nanoclusters are observed on the terrace sites of a  $\text{SiO}_2$  thin film prepared at a lower annealing temperature. A plot of the number density of Au clusters with respect to Au coverage shows that the nucleation and growth of Au clusters is initially dominated by oxygen vacancy complexes.

**Acknowledgment.** We acknowledge with pleasure the support of this work by U.S. Department of Energy, Office of Basic Energy Science, Division of Chemical Sciences, the

Robert A. Welch Foundation, and the Texas Advanced Technology Program under Grant no. 010366-0022-2001.

### References and Notes

- (1) Franchy, R. *Surf. Sci. Rep.* **2000**, *38*, 195 and references therein.
- (2) Valden, M.; Lai, X.; Goodman, D. W. *Science* **1998**, *281*, 5383.
- (3) Wahlstrom, E.; Lopez, N.; Schaub, R.; Thosttrup, P.; Ronnau, A.; Africh, C.; Laegsgaard, E.; Norskov, J. K.; Besenbacher, F. *Phys. Rev. Lett.* **2003**, *90*, 026101.
- (4) Haas, G.; Menck, A.; Brune, H.; Barth, J. V. *Phys. Rev. B* **2000**, *61*, 11105.
- (5) Bogicevic, A.; Jennison, D. R. *Surf. Sci.* **2002**, *515*, L481.
- (6) Bäumer, M.; Frank, M.; Heemeier, M.; Kuhnemuth, R.; Stempel, S.; Freund, H.-J. *Surf. Sci.* **2000**, *454–456*, 957.
- (7) Bäumer, M.; Freund, H.-J. *Prog. Surf. Sci.* **1999**, *61*, 127.
- (8) Min, B. K.; Santra, A. K.; Goodman, D. W. *J. Vac. Sci. B* **2003**, *21*, 2319.
- (9) Kim, Y. D.; Wei, T.; Goodman, D. W. *Langmuir* **2003**, *19*, 354.
- (10) Lai, X.; St Clair, T. P.; Valden, M.; Goodman, D. W. *Prog. Surf. Sci.* **1998**, *59*, 25.
- (11) Ozensoy, E.; Min, B. K.; Santra, A. K.; Goodman, D. W. *J. Phys. Chem. B* **2004**, *108*, 4351.
- (12) Wendt, S.; Kim, Y. D.; Goodman, D. W. *Prog. Surf. Sci.* **2003**, *74*, 141.
- (13) Min, B. K.; Wallace, W. T.; Goodman, D. W. *J. Phys. Chem. B* **2004**, *108*, 14609.
- (14) Henrich, V. E.; Cox, P. A. *The surface science of metal oxides*; Cambridge University Press: Cambridge, U.K., 1994.
- (15) Kulawik, M.; Nilius, N.; Rust, H.-P.; Freund, H.-J. *Phys. Rev. Lett.* **2003**, *91*, 256101–1.
- (16) Pacchioni, G.; Ierano, G. *Phys. Rev. B* **1998**, *57*, 818.
- (17) Eitel, W. *The Physical Chemistry of the Silicates*; University of Chicago Press: Chicago, 1954.
- (18) Schroeder, T.; Giorgi, J. B.; Bäumer, M.; Freund, H.-J. *Phys. Rev. B* **2002**, *66*, 165422.
- (19) Schroeder, T.; Hammoudeh, A.; Pykavy, M.; Magg, N.; Adelt, M.; Bäumer, M.; Freund, H.-J. *Solid-State Electron.* **2001**, *45*, 1471.
- (20) Bermudez, V. M.; Ritz, V. H. *Phys. Rev. B* **1979**, *20*, 3446.
- (21) Namai, Y.; Fukui, K.-I.; Iwasawa, Y. *J. Phys. Chem. B* **2003**, *107*, 11666.